Spectrochimica Acta Part A 77 (2010) 297–303

Contents lists available at ScienceDirect

Spectrochimica Acta Part A: Molecular and Biomolecular Spectroscopy

journal homepage: www.elsevier.com/locate/saa

Ligational, analytical and biological applications on oxalyl bis(3,4-dihydroxybenzylidene) hydrazone

Ahmed A. El-Asmy*, O.A. El-Gammal, H.A. Radwan, S.E. Ghazy

Chemistry Department, Faculty of Science, Mansoura University, Mansoura, Dakhalia 35516, Egypt

ARTICLE INFO

Article history:
Received 23 March 2010
Received in revised form 11 May 2010
Accepted 15 May 2010

Keywords:
Oxalyl bis(3,4-dihydroxybenzylidene) hydrazone
Flotation
Spectra
Cr^{3+}, VO^{2+}, ZrO^{2+}, HfO^{2+}, UO_2^{2+} and MoO_2^{2+} complexes

ABSTRACT

The molecular modeling and parameters have been calculated to confirm the geometry of oxalyl bis(3,4-dihydroxybenzylidene) hydrazone, H_6L. The metal complexes of Cr^{3+}, VO^{2+}, ZrO^{2+}, HfO^{2+}, UO_2^{2+} and MoO_2^{2+} with H_6L have been prepared and characterized by partial elemental analysis, spectral studies (electronic; IR), thermal analysis and magnetic measurements. The data suggest the formation of polymer complexes with a unit $[Cr(H_4L)(H_2O)_3Cl]\cdot H_2O$, $[VO(H_4L)(H_2O)_2]$, $[Hf(H_4L)(H_2O)]\cdot H_2O$ $[UO_2(H_4L)(H_2O)_2]\cdot 2H_2O$ $[MoO_2(H_4L)]$ and $[(ZrO)_2(H_2L)\text{-}(C_2H_5OH)_2]$. The ligand behaves as a dibasic bidentate in all complexes except ZrO^{2+} which acts as a tetrabasic tetradentate with the two ZrO^{2+} ions. An octahedral geometry was proposed for the Cr^{3+}, HfO^{2+}, $MoO_2^{2+}$and UO_2^{2+} complexes and square pyramid for VO^{2+}. The Cr^{3+} is necessary to degrade the DNA of eukaryotic subject completely; the other complexes have little effect. H_6L was found suitable as a new reagent for the separation and preconcentration of ZrO^{2+} ions from different water samples using flotation technique with satisfactory results.

1. Introduction

The synthesis and structural characterization of metal complexes of hydrazones have much interest to compare their coordinative behavior with their antimicrobial activities. Copper(II) complexes of certain hydrazones have antitumor activity [1]. Diacetylmonoxime thiosemicarbazone is effective against vaccinia infections in mice by chelating some essential metal ions from the virus [2]. Oximinohydrazones have antiparasitic, fungicidal and bactericidal properties [3]. Compounds containing oxime and amino groups are used as analytical reagents for the microdetermination of some transition metal ions and as ion exchange resins [4]. Series of pyridazinyl hydrazones were found to inhibit *tyrosine hydroxylase* and *dopamine hydroxylase in vivo* and *in vitro* [5]. Tridentate hydrazones have been evaluated as potential oral iron-chelating drugs for genetic disorders such as thalassemia [6]. The X-ray crystal structure of the ferric complex of pyridoxalisonicotinoyl hydrazone showed that the ligand acts as a tridentate planar chelating agent with the remaining sites around the iron occupied by chloride ions or water molecules [7]. Salicylaldehydebenzoyl hydrazone appeared to be unusually potent inhibitor of DNA synthesis and cell growth in a variety of human and rodent cell lines [8]. The complexes of Cu(II), Co(II), Ni(II), Mn(II), Ce(III) and UO_2^{2+} with 2-aceto-1-naphthol-N-salicoyl hydrazone have been prepared and characterized. The 1:2 (M:L) complexes of Cu(II), Ni(II), Co(II) and Mn(II) have an octahedral structure while 1:1 of Cu(II) and Ni(II) are square planar. The ligand was used for the microdetermination of metal ions in solution [9].

Binuclear complexes of VO^{2+}, Co^{2+}, Ni^{2+}, Cu^{2+} and Zn^{2+} with oxalyl bis(diacetylmonoxime hydrazone) were prepared. The data suggest a 2:2 (M:L) molar ratio. An octahedral geometry for VO^{2+} complex, tetrahedral for Zn^{2+} and square planar for the rest complexes were proposed [10]. Complexes of UO_2^{2+}, VO^{2+} and ZrO^{2+} ions with vitamin B_{13} (orotic acid) were reported and formulated as: $[M(C_5H_3N_2O_4)_2(H_2O)_2]\cdot(H_2O)_n$. The antibacterial activity of orotic acid and its complexes were tested against gram positive/negative bacteria [11]. 2,5-Dihydroxyacetophenone-isonicotinoyl hydrazone (H_2L) was synthesized as well as its metal complexes with Cr^{3+}, Mn^{3+}, Fe^{3+}, VO^{2+}, Zr^{4+} and UO_2^{2+}. The Schiff base behaved as a flexidentate ligand and commonly coordinated through the oxygen atom of the deprotonated phenolic group and the azomethine nitrogen. The thermal data were analyzed for the kinetic parameters. All the compounds were screened for their antimicrobial activity by agar cup-plate method against various organisms and the results compared [12]. Series of mono and binuclear Mn^{2+}, Fe^{3+}, Co^{2+}, Ni^{2+}, Cu^{2+}, Zn^{2+}, La^{3+}, Ru^{3+}, Hf^{4+}, ZrO^{2+} and UO_2^{2+} complexes of phenylamino-dibenzoyl hydrazone were synthesized and characterized [13].

Up to date, no work on complexes containing Cr^{3+}, VO^{2+}, ZrO^{2+}, HfO^{2+}, UO_2^{2+} and MoO_2^{2+} ions with the investigated ligand, H_6L.

* Corresponding author. Tel.: +20 101645966; fax: +20 502236787.
E-mail address: aelasmy@yahoo.com (A.A. El-Asmy).

1386-1425/$ – see front matter © 2010 Elsevier B.V. All rights reserved.
doi:10.1016/j.saa.2010.05.026

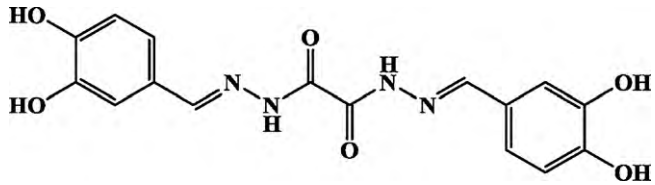

Scheme 1. Formula of H_6L.

2. Experimental

$VOSO_4{\cdot}2H_2O$, $CrCl_3{\cdot}3H_2O$, $ZrCl_4$, $HfCl_4$, $UO_2(OAc)_2$ and $(NH_4)_2MoO_4$, diethyl oxalate, hydrazine hydrate, 3,4-dihydroxybenzaldehyde, ethanol, diethyl ether, DMF and DMSO were obtained from the BDH chemicals.

2.1. Synthesis of H_6L

Oxalyl bis(3,4-dihydroxybenzylidene) hydrazone, Scheme 1, was prepared by heating a suspension (6 g, 0.05 mol) of oxalic acid dihydrazide ($NH_2NHCOCONHNH_2$) in 20 mL EtOH with 13.8 g (0.1 mol) of 3,4-dihydroxybenzaldehyde in 10 mL EtOH on a water bath for 1 day. Complete reaction is tested by thin layer chromatography (TLC) in petroleum ether-ethyl acetate (1:2) as eluent. It gives one spot with Rf = 0.34. The precipitate was filtered off, recrystallized from ethanol and dried; the yield is 79%. The ligand was characterized by spectral studies and elemental analysis. The ^1H NMR spectrum of the ligand gives different signals at δ = 12.05, 9.48, 7.41–6.85 and 2.32 ppm corresponding to the protons of OH, NH, aromatic CH and aliphatic CH, respectively.

2.2. Preparation of complexes

The solid complexes were prepared by reacting the calculated amounts for 2:1 ratio [M:L] of metal salt and ligand in H_2O–EtOH (v/v) solution and the mixture was heated under reflux on a water bath for 6–8 h. In the preparation of VO^{2+} complex, 0.1 g of sodium acetate was added. The precipitate thus formed was filtered off, washed with hot water, hot ethanol and diethyl ether and finally dried in a vacuum desiccator over anhydrous $CaCl_2$.

2.3. Flotation method

A 3 mL aliquot containing 0.5×10^{-5} mol L^{-1} ZrO^{2+} was mixed with H_6L (1×10^{-4} mol L^{-1}) and 3 mL bidistilled water. The pH was adjusted at ~3. The solution was then transferred quantitatively to the flotation cell and completed to 10 mL with bidistilled water. The cell was shaken well for few seconds to ensure complete complexation. To this solution, 3 mL of 1.0×10^{-5} mol L^{-1} HOL were added and the cell was then inverted upside down many times by hand. After complete separation, the scum containing ZrO^{2+}–H_6L complex was separated, eluted with 4 mL of 4 M HCl, diluted to 10 mL in a volumetric flask and subjected to spectral determination.

2.4. Antibacterial and genotoxicity studies

H_6L and metal complexes were screened for their antimicrobial activity using Gram positive (BT) and Gram negative bacteria (*E. coli*). The media prepared for bacteria were as reported earlier [14]. For a genotoxicity study, a solution of 2 mg of Calf thymus DNA was dissolved in 1 mL of sterile distilled water where the investigated ligand and its complexes were prepared by dissolving 2 mg mL^{-1} DMSO. An equal volume of each compound and DNA were mixed thoroughly and kept at room temperature for 2–3 h. The effect of the compounds on the DNA was analyzed by agarose gel electrophoresis. A 2 μL of loading dye were added to 15 μL of the DNA mixture before being loaded into the well of an agarose gel. The loaded mixtures were fractionated by electrophoresis, visualized by UV and photographed.

2.5. Equipment and analysis

C, H and N contents of H_6L and complexes were determined at the Microanalytical Unit of Cairo University, Egypt. The metal content was determined by gravimetric or complexometric methods [15]. The IR spectra were recorded as KBr disc on a Mattson 5000 FTIR Spectrophotometer (200–4000 cm^{-1}). The UV–vis spectra of the complexes were recorded on UV_2 Unicam Spectrophotometer (200–900 nm). The ^1H NMR spectrum of the ligand was recorded in deuterated dimethulsulphoxide (DMSO-d6), on a Bruker WP 200 SY spectrometer (300 MHz) at room temperature using tetramethylsilane (TMS) as an external standard. The magnetic measurements were carried out on a Johnson-Matthey magnetic balance, UK. Thermogravimety (TGA) was measured (20–800 °C) on a Shimadzu TGA-50; the nitrogen flow and heating rate were 20 mL min^{-1} and 10 °C min^{-1}, respectively. ESR spectra were obtained on a Bruker EMX spectrometer working in the X-band (9.78 GHz) with 100 kHz modulation frequency. The microwave power was set at 0.004. A powder spectrum was obtained in a 2 mm quartz capillary at room temperature.

All molecular calculations were carried out by HyperChem 7.51 software package. The molecular geometry of the ligand and its ZrO^{2+} complex is first optimized at molecular mechanics (MM+) level. Semi-empirical method PM3 is then used for optimizing the full geometry of the system using Polak–Ribiere (conjugate gra-

Table 1
Color, melting points and partial elemental analyses of H_6L and its complexes.

Compound	Color	M.P. (°C)	% Found (calcd.)			
			C	H	N	M
H_6L $C_{16}H_{14}N_4O_6$, 358.32	Pale yellow	295–96	53.2 (53.6)	5.5 (5.9)	14.9 (15.6)	–
$[VO(H_4L)(H_2O)_2]$ $C_{16}H_{16}N_4O_7V$, 459.27	Brownish green	>300	42.2 (41.8)	3.7 (3.5)	12.6 (12.2)	11.4 (11.1)
$[Cr(H_4L)(H_2O)_3Cl]H_2O$ $C_{16}H_{20}N_4O_{10}CrCl$, 516.73	Brown	>300	36.8 (37.2)	3.7 (3.9)	10.4 (10.8)	10.5 (10.1)
$[(ZrO)_2(H_2L)(C_2H_5OH)_2]$ $C_{20}H_{22}N_4O_{10}Zr_2$, 660.83	Yellowish orange	>300	37.0 (36.4)	4.0 (3.6)	8.1 (8.5)	31.9 (32.4
$[HfO(H_4L)(H_2O)]H_2O$ $C_{16}H_{14}N_4O_8Hf$, 586.84	Brownish orange	>300	33.2 (32.7)	3.1 (2.7)	9.2 (9.5)	
$[MoO_2(H_4L)]$ $C_{16}H_{12}N_4O_8$, 483.91	Brownish green	>300	39.3 (38.8)	3.8 (4.2)	11.8 (11.6)	
$[UO_2(H_4L)(H_2O)_2]2H_2O$ $C_{16}H_{20}N_4O_{12}U$, 698.45	Brown	>300	26.9 (27.5)	3.3 (2.9)		34.5 (34.1)

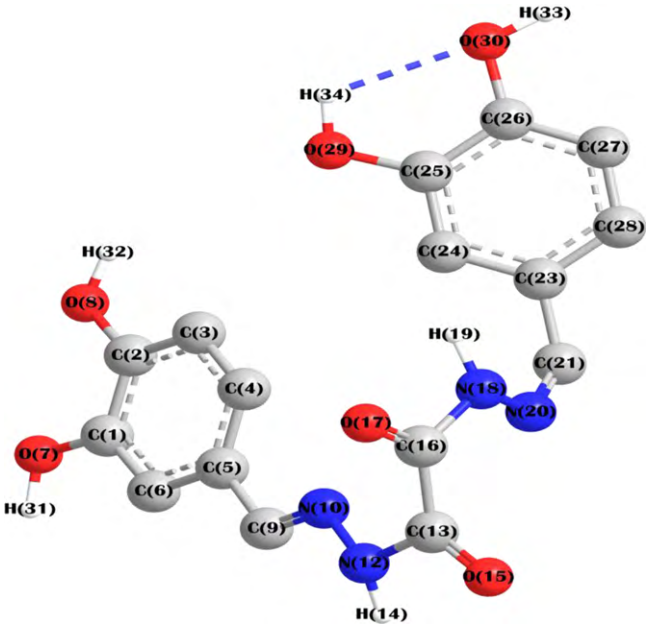

Scheme 2. Molecular modeling of H_6L.

dient) algorithm and Unrestricted Hartee-Fock (UHF) is employed keeping RMS gradient of 0.01 kcal (Å mol^{-1}).

3. Results and discussion

3.1. General

The color, melting points and elemental analyses of the complexes are compiled in Table 1. The data are in agreement with the formulae $[Cr(H_4L)(H_2O)_3Cl]\cdot H_2O$, $[M(H_4L)(H_2O)_n]\cdot mH_2O$ (M = VO, HfO, MoO_2 or UO_2) and $[(ZrO)_2(H_2L)(C_2H_5OH)_2]$. The complexes are insoluble in most common organic solvents and partially soluble in dimethylformamide (DMF) and DMSO. The partial solubility of the complexes in DMSO or DMF prevents the growing of crystals for X-ray crystallography and the measurement of their molar conductances and ^1H NMR spectra. The intense color may be due to a charge transfer or a defect of crystal during the preparation. HfO^{2+} complex have more intense color than ZrO^{2+} complex which may be due to high polarization; the band at 14,680 cm^{-1} in its electronic spectrum is due to ligand–metal charge transfer (LMCT). The thermal analyses indicate high stability for some complexes; a behavior consistent with a polymeric nature of the complexes.

3.2. Molecular modeling of H_6L

The molecular numbering of H_6L is shown in Scheme 2. Analysis of the data in Tables 1S and 2S calculated for both length and angle for each bond, one can conclude the following remarks: (i) all bond lengths of the O–H and C–O are nearly similar, except C(16)–O(17) and C(13)–O(15) which are smaller than the rest due to the double bond character; (ii) the two N–N bond lengths are typical; they surround with similar substituents; (iii) all bond angles predict sp^3 and sp^2 hybridization; (iv) the bond angles of C(21)–N(20)–N(18), O(17)–C(16)–C(13) and C(16)–C(13)–O(15) are 123.39, 123.35 and 124.87 while C(23)–C(21)–N(20) is 127.39°.

The calculated total energy; binding energy; electronic energy and heat of formation are −1,041,311; −4295; −740,887 and −22 kcal mol^{-1}, respectively, dipole moment = 3.144 D; HOMO = −8.773392 eV and LUMO = −0.3302211 eV.

3.3. IR spectra of H_6L and complexes

The IR spectrum of H_6L showed bands at 3486, [2363(w), 2338(w)], 3374(w), 1653(vs), 1612(s), 1517(w) and 1366(s) due to the $\nu(OH)_{free}$, $[\nu(OH)_{bonded}]$, ν(NH), ν(C=O), ν(C=N), amide II [δ(N–H) + ν(C=N)] and δ(OH) vibrations, respectively. The bands at 2363 and 2338 cm^{-1} exist at more less wavenumbers than the free indicating strong O–H···O hydrogen bonding [16].

The absence of the OH bands (Table 2) in the spectra of all complexes indicates the destruction of the hydrogen bond during complexation and instead another band appears at 3396–3442 cm^{-1} in the spectra of all complexes, except for the ZrO^{2+} complex, indicating the involvement of two OHs in chelation; the other two are still protonated with weak hydrogen bond. In the ZrO^{2+} complex, no band in this region confirming the involvement of the four OHs in coordination. Another support for the OH coordination is the appearance of the δ(OH) band at 1366 cm^{-1} with low intensity as well as new one at 1338 cm^{-1} duo to the δ(OH) of the coordinated water. Ethanol in the zirconyl complex is supported by the appearance of δ(OH) strong. The ν(NH), ν(C=O) and ν(C=N) bands appeared more or less at the same position as in the spectrum of H_6L indicating no chelation through these groups; these groups exist opposite to each other (from molecular calculation). Also, the IR spectra of the complexes showed a new band at 464–521 cm^{-1} due to ν(M–O) vibration. The vanadyl complex showed a strong band, at 970 cm^{-1}, attributed to the ν(V=O) vibration which is an evidence for the square-pyramidal configuration of the VO^{2+} complex [17].

The IR spectrum of $[UO_2(H_4L)(H_2O)_2]\cdot 2H_2O$ displayed two bands at 929 and 873 assigned to ν_3 and ν_1 of the dioxouranium ion (Scheme 2). The force constant (F_{U-O} = 7.125 mdynes $Å^{-1}$) of the U=O bond is calculated by [18]: $(\nu_3)^2 = (1307)^2\,(F_{U-O})/14.103$. Substituting its value in the Jones relation [19]: $R_{U-O} = 1.08\,(F_{U-O})^{-1/3} + 1.17$, R_{U-O} was 1.73 Å. These values falling within the usual range for the uranyl complexes (Scheme 3).

MoO_2^{2+} complex showed bands at 904 and 850 cm^{-1}. Using the same above equations, F_{Mo-O} and R_{Mo-O} for O=Mo=O are 6.75 mdynes $Å^{-1}$ and 1.74 Å, respectively. Mo–O radius is approximately similar to U–O.

The broad bands at ~3360, ~890 and ~540 cm^{-1} in the spectra of $[VO(H_4L)(H_2O)_2]$, $[Cr(H_4L)(H_2O)_3Cl]\cdot H_2O$ and $[UO_2(H_4L)(H_2O)_2]\cdot 2H_2O$ are attributed to υ(OH), $\rho_r(H_2O)$ and

Table 2
Assignments of the IR spectral bands of H_6L and its complexes.

Compound	ν(OH)	ν(NH)	ν(C=O)	ν(C=N)	[δ(N–H) + ν(C–N)]	δ(OH)	ν(M–O)
H_6DPOH	3486, 2363, 2338	3374	1653	1612	1517	1367	–
$[VO(H_4L)(H_2O)_2]$	3396, –	3242	1644	1593	1517	1366	468
$[Cr(H_4L)(H_2O)_3Cl]H_2O$	3343, –	3247	1653	1611	1517	1337[a], 1366	470
$[(ZrO)_2(H_2L)(C_2H_5OH)_2]$	–	3247	1656	1614	1515	1365[a]	466
$[HfO(H_4L)(H_2O)]H_2O$	3442, –	3247	1656	1614	1515	1338[a], 1359	464
$[UO_2(H_4L)(H_2O)_2]2H_2O$	3344, –	3247	1653	1607	1516	1369	467
$[MoO_2(H_4L)]$	3419, –	3180	1679	1589	1530	1372	521

[a] δ(OH) of the coordinated water.

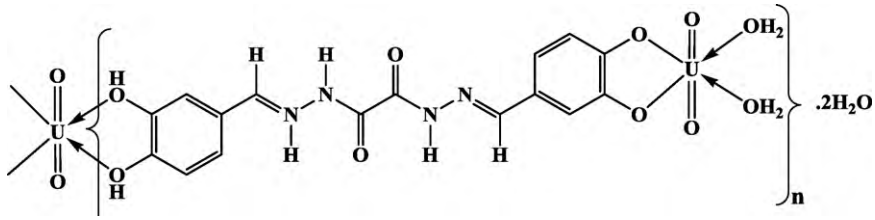

Scheme 3. Structure of $[UO_2(H_4L)(H_2O)_2]\cdot 2H_2O$.

Table 3
Magnetic moments and electronic spectral bands of the compounds.

Compound	μ_{eff} (BM)	State	Intraligand and charge transfer (cm^{-1})	d–d transition (cm^{-1})
H_6L	–	DMF	35,740; 33,000; 32,050; 27,900; 26,455	–
$[(ZrO)_2(H_2L)(C_2H_5OH)_2]$	–	DMF	36,765; 32,680; 29,410; 27,470	–
$[Cr(H_4L)(H_2O)_3Cl]H_2O$	3.69	DMF	35,970; 32,895	22,830; 21,830; 18,050; 16,450
$[UO_2(H_4L)(H_2O)_2]2H_2O$	–	DMSO	35,710; 33,110; 27,860; 24,340	–
$[MoO_2(H_4L)]$	–	NujolDMF	34,720; 31,650; 27,625; 26,040 × 33,110;28,250; 24,040; 19,840	–
$[VO(H_4L)(H_2O)_2]$	1.74	Nujol	33,110; 28,250; 23,920	19,840
$[HfO(H_4L)(H_2O)]H_2O$	–	Nujol	24,330; 22,330; 21,190; 14,640	–

$\rho_w(H_2O)$, respectively, confirming water of coordination [20]; these bands absent in the rest complexes.

3.4. Electronic and magnetic studies

The magnetic moment values of the VO^{2+} and Cr^{3+} complexes are 1.74 and 3.57 BM, consistent with the presence of one and three unpaired electrons. The other complexes have a diamagnetic nature in accordance with the d^0 or d^{10} configuration.

The spectrum of H_6L showed $\pi \rightarrow \pi^*$ and $n \rightarrow \pi^*$ bands at 35,740–26,455 cm^{-1}. Changes are observed on the spectra of its complexes (Table 3).

The electronic spectrum of $[Cr(H_4L)(H_2O)_3Cl]\cdot H_2O$ (Fig. 1) showed two strong absorption bands at 18,050 and 22,831 cm^{-1} attributed to the $^4A_{2g}$ (F) → $^4T_{2g}$ (P) and $^4A_{2g}$ (F) → $^4T_{1g}$ (F) transitions, in an octahedral geometry. An additional broad band centered at 24,210 cm^{-1} is due to a charge transfer. The ligand field parameters (Dq = 1805 cm^{-1}, B = 429.8 cm^{-1} and β = 0.46) are further support for the proposed geometry. The lower value of β indicates more covalency. The two bands at 23,920 and 19,840 cm^{-1} in $[VO(H_4L)(H_2O)_2]$ are assigned to the $d_{xz} \rightarrow d_{xy}$ transition in a square-pyramidal geometry [21]. The color and IR band support square-pyramid structure (Scheme 4).

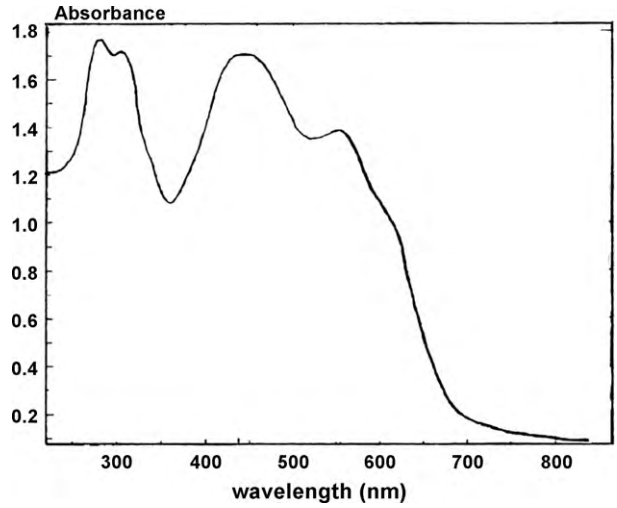

Fig. 1. Electronic spectrum of $[Cr(H_4L)(H_2O)_3(Cl)]\cdot H_2O$.

The spectrum of $[UO_2(H_4L)(H_2O)_2)]\cdot 2H_2O$ showed a band at 24,340 cm^{-1} similar to the O=U=O symmetric stretching frequency for the first excited state [22].

The electronic spectrum of $[MoO_2(H_4L]$ in Nujol (DMF) showed bands at 34,720 (33,110), 31,650, 27,625 (28,250) and 26,040 (24,040) cm^{-1} which are more or less similar to those in the ligand spectrum. The band at 24,040 cm^{-1} is similar to that in the UO_2 spectrum indicating O=Mo=O moiety. The shoulder at 19,840 cm^{-1} in DMF spectrum arising from O pseudo-sigma combinations to the singly occupied Mo 4d orbital in the *xy* plane suggesting a considerable covalency in the ground-state electronic structure of $[MoO_2(H_4L)]_n$ (Scheme 5). There is no evidence for any d–d transition and the data cast no doubt about the six coordination of the complex [23,24].

3.5. Thermal analysis

The thermogravimetric curves (25–800 °C) of some complexes were recorded to give an insight into the thermal stability of the studied complexes. In Cr^{3+} and HfO^{2+}, the first decomposition step is due to the loss of water of crystallization in the temperature range 40–150 °C. In the other complexes, the first decomposition step begins at 205, 207 and 268 °C.

The TG curve of $[VO(H_4L)(H_2O)_2]$ (Fig. 2) displayed a thermal stability till 205 °C, after which five degradation steps were observed at 205–285, 286–353, 355–434, 435–515 and 516–730 °C. The first

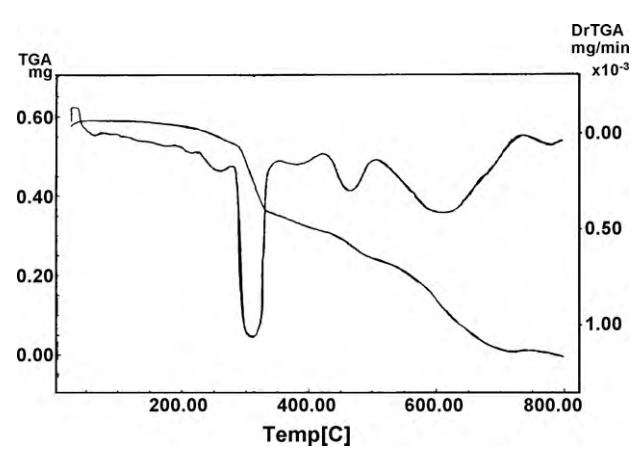

Fig. 2. Thermal analysis curves (TGA, DTA) of $[VO(H_4L)(H_2O)_2]$.

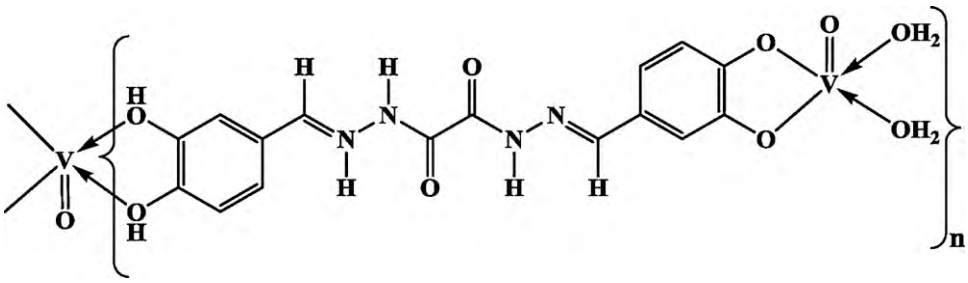

Scheme 4. Structure of $[VO(H_4L)(H_2O)_2]$.

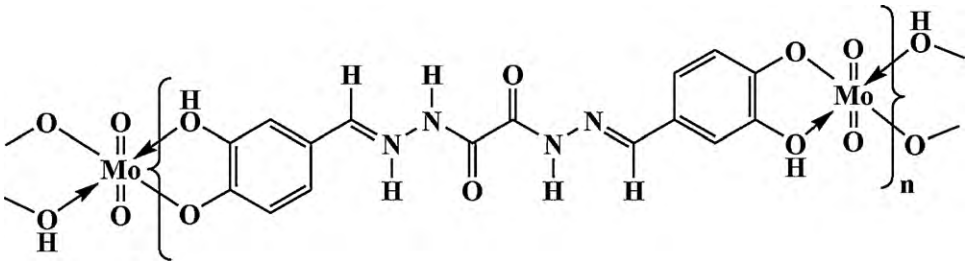

Scheme 5. Structure $[MoO_2(H_4L]$.

step is due to the removal of $2H_2O$ with 8.0 (calcd. 7.8%) weight loss. $C_7H_4NO_2VO$ still exists in the last step by 40.7 (calcd. 40.9%) revealing a high stability of the final species at 730 °C.

In $[(ZrO)_2(H_2L)(C_2H_5OH)_2]$, the decomposition begins at 268 °C indicating a high stability of the complex. The first step at 269–362 °C is due to the removal of $2C_2H_5OH + C_4H_2O_2$. The final step ending at 800 °C is corresponding to Zr_2O_3.

The TGA curve of $[MoO_2(H_4L)]$ (Fig. 3) showed four degradation steps. At 30–376 °C, the $C_7H_7N_2O_2$ fragment is removed with weight loss of 30.5 (calcd. 31.2%). The second step ended at 516 °C is corresponding to the loss of $C_4H_2O_2N_2$ with 22.2 (22.7%). The third step ending at 591 °C is corresponding to the removal of CH with 2.7 (calcd. 4.3%). The residue at 591–800 °C [43.3 (calcd. 44.4%)] is $[MoO_2(C_4H_3O_2)]$. Equations representing the degradation steps for the complexes are:

$$[VO(C_{16}H_{14}N_4O_6)(H_2O)_2] \rightarrow [VO(C_{16}H_{14}N_4O_6)] + \{2H_2O\}$$
$$\rightarrow [VO(C_9H_8N_3O_4)] + \{C_7H_6NO_2\}$$
$$\rightarrow [VO(C_8H_7N_2O_3)] + \{CONH\}$$
$$\rightarrow [VO(C_7H_6O_2)] + \{CHN_2O\}$$

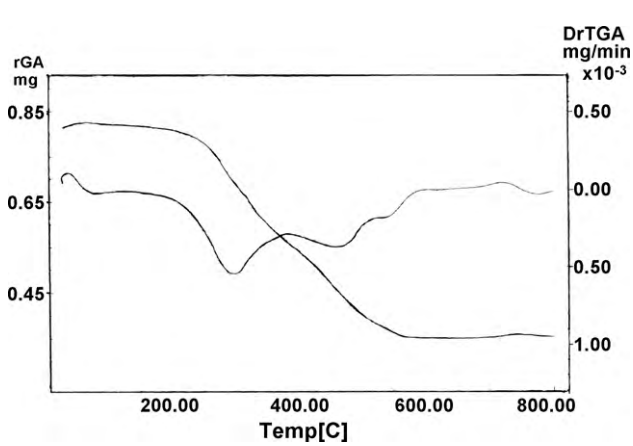

Fig. 3. Thermal analysis curves (TGA, DTA) of $[MoO_2(H_4L)]$.

$$[Cr(C_{16}H_{12}N_4O_6)(H_2O)_3Cl]H_2O$$
$$\rightarrow [Cr(C_{16}H_{12}N_4O_6)(H_2O)_2Cl] + \{2H_2O\}$$
$$\rightarrow [Cr(C_{14}H_{10}N_2O_4)Cl] + \{C_2H_2N_2O_2 + 2H_2O\}$$
$$\rightarrow [Cr(C_3HO_2)] + \{(C_{11}H_9N_2O_2Cl)\}$$

$$[(ZrO)_2(C_{16}H_{10}N_4O_6)(C_2H_5OH)_2]$$
$$\rightarrow [(ZrO)_2(C_{14}H_8N_2O_4)] + \{2C_2H_5OH + C_2H_2N_2O_2\}$$
$$\rightarrow [(ZrO)_2(N_2O_4)] + \{C_{14}H_8\} \rightarrow Zr_2O_2 + \{N_2O_4\}$$

$$[HfO(C_{16}H_{12}N_4O_6)(H_2O)]\cdot H_2O$$
$$\rightarrow [HfO(C_{16}H_{12}N_4O_6)(H_2O)] + \{H_2O\}$$
$$\rightarrow [HfO(C_{14}H_{10}N_2O_4)] + \{H_2O + C_2H_2N_2O_2\}$$
$$\rightarrow [HfO(C_{13}H_9NO_4)] + \{CNH\}$$
$$\rightarrow [HfO(C_7H_6NO_4)] + \{C_6H_3\} \rightarrow [HfO(C_7H_4NO_2)] + \{H_2O_2\}$$

$$[MoO_2(C_{16}H_{13}N_4O_6)] \rightarrow [MoO_2(C_9H_6N_2O_4)] + \{C_7H_7N_2O_2\}$$
$$\rightarrow [MoO_2(C_5H_4O_2)] + \{C_4H_2O_2N_2\}$$
$$\rightarrow [MoO_2(C_4H_3O_2)] + \{CH\}$$

3.6. *ESR spectrum of $[VO(C_{16}H_{14}N_4O_6)(H_2O)_2]$*

The ESR spectra of the vanadyl complexes provide information about hyperfine and superhyperfine structures. Generally, the mononuclear VO^{2+} ion (S = 1/2, I = 7/2) has a characteristic octet ESR spectrum showing the hyperfine coupling to the ^{51}V nuclear magnetic moment. The superexchange interaction between the two vanadium ions lead to a configuration in which the two electron spins have an antiferromagnetic character [25]. Therefore, the ESR spectrum of strongly coupled pairs has the form of a single broad line with inhomogeneous broadening. V(IV) complexes generally have *g*-values less than 2.0023.

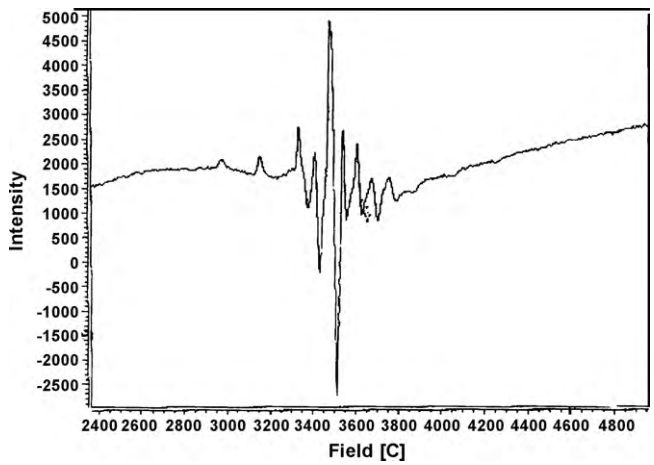

Fig. 4. The ESR spectrum of $[VO(H_4L)(H_2O)_2]$.

The room temperature (300 K) ESR spectrum of $[VO(H_4L)(H_2O)_2]$ gave a typical eight-line pattern (Fig. 4) similar to those reported for mononuclear vanadium molecule [26]. The spectra of mono vanadium complexes showed the parallel and perpendicular features which indicate axially symmetric anisotropy with well resolved sixteen-lines hyperfine splitting characteristic for the interaction between the electron and the vanadium nuclear spin (I = 7/2) [27]. The spin Hamiltonian parameters are calculated to be $g_{//}$ (1.93), $g_{\perp}$ (1.97), $A_{//}$ (190×10^{-4} cm^{-1}) and $A_{\perp}$ (60). The calculated ESR parameters indicate that the unpaired electron (d^1) is present in the d_{xy}-orbital with square-pyramidal or octahedral geometry [28]. The values obtained agree well with the *g*-tensor parameters reported for square pyramidal geometry [29].

The molecular orbital coefficients α^2 and β^2 for $[VO(H_4L)(H_2O)_2]$ were calculated using the reported equations [30] and found to be 0.93 and 0.77, respectively. The lower value of β^2 indicates that the in-plane σ-bonding is less covalent and well consistent with other reported data [29].

3.7. Molecular modeling of $[(ZrO)_2(H_2DPOH)(C_2H_5OH)_2]$

The molecular parameters of $[(ZrO)_2(H_2DPOH)(C_2H_5OH)_2]$ (Scheme 6) are calculated to be: total energy = −155,902; binding energy = −6443; electronic energy = −1,262,984; heat of formation = 10.1 kcal mol^{-1}; dipole moment = 18.233 D; HOMO = −8.1334 eV and LUMO = −0.9909 eV. The bond lengths and the bond angles are presented in Tables 3S and 4S.

3.8. Eukaryotic DNA degradation test

Examining the DNA degradation assay of H_6DPOH and its metal complexes revealed variability on their immediate damage on the calf thymus (CT) DNA. The complexes have a high effect than the ligand; VO^{2+} and ZrO^{2+} complexes degraded the CT DNA completely. The results suggest that direct contact of VO^{2+} and ZrO^{2+} is necessary to degrade the DNA of eukaryotic subject.

The ligand and its metal complexes have been tested against Gram positive (BT) and Gram negative bacteria (*E. coli*). All compounds have small inhibitory effects on bacteria.

3.9. Separation and determination of ZrO^{2+} using H_6L

Different factors affecting the flotation of ZrO^{2+} using H_6L have been studied to maximize its separation efficiency. The most important are:

pH: A series of experiments were carried out to show the effect of HCl and/or NaOH on the separation of 0.5×10^{-4} mol L^{-1} ZrO^{2+}, in the presence of 1×10^{-5} mol L^{-1} oleic acid (HOL) and 1×10^{-4} mol L^{-1} H_6L. The results show that the floatability of ZrO^{2+}–H_6L increases with increasing the pH, reaching a maximum at 2.5–3.5. Therefore, all work experiments were carried out at pH ~3.

Ligand concentration: Trials were performed to float ZrO^{2+} with oleic acid individually; the efficiency does not exceed 35%. H_6DPOH was the reagent added to give good results. The floatability of a series of solutions containing 0.5×10^{-4} mol L^{-1} ZrO^{2+}, 1×10^{-5} mol L^{-1} HOL and various amounts of H_6L at pH ~3 was performed. The results show a maximum efficiency (98.4%) at 1:2 ($ZrO:H_6L$) ratio. Excess ligand has no effect, so the procedure find application for real samples containing ZrO^{2+}. A concentration of H_6L equals two-folds of ZrO^{2+} or more was used.

Surfactant concentration: ZrO^{2+} was separated using various concentrations of HOL. The results show maximum floatability at 1×10^{-5}–3.36×10^{-2} mol L^{-1} of HOL, above which the flotation decreases. Accordingly, 1×10^{-5} mol L^{-1} HOL was the desired concentration.

ZrO^{2+} concentration: Various amounts of ZrO^{2+} were floated in the presence of 1×10^{-4} mol L^{-1} H_6L using 1×10^{-5} mol L^{-1} HOL at pH ~3. The floatability reaches 98.2% at 0.5×10^{-4} mol L^{-1} of ZrO^{2+} corresponding to $ZrO:2H_6L$. At higher concentration of ZrO^{2+}, the efficiency decreases and needs excess H_6L.

Temperature: Solutions of ZrO^{2+}, H_6L and HOL were either heated or cooled; the HOL was quickly poured into the mixture and introduced into the flotation cell jacketed with 1 cm thick fiberglass. The floatability does not affected by temperature (0–70 °C). Since the industrial waste waters are usually hot, the introduced procedure finds successful application in the direct analysis of ZrO^{2+} ions wastes. The subsequent measurements were carried out at room temperature ~30 °C.

Foreign ions: Separation of 0.5×10^{-4} mol L^{-1} ZrO^{2+} using 1×10^{-4} mol L^{-1} H_6L and oleic acid (1×10^{-5} mol L^{-1}) was carried out at high concentrations of various cations and anions usually found in some water samples (Table 4). Tolerable amount (presented as ion:ZrO ratio) giving a maximum error of ±2% in the flotation efficiency. All investigated ions do not interfere except

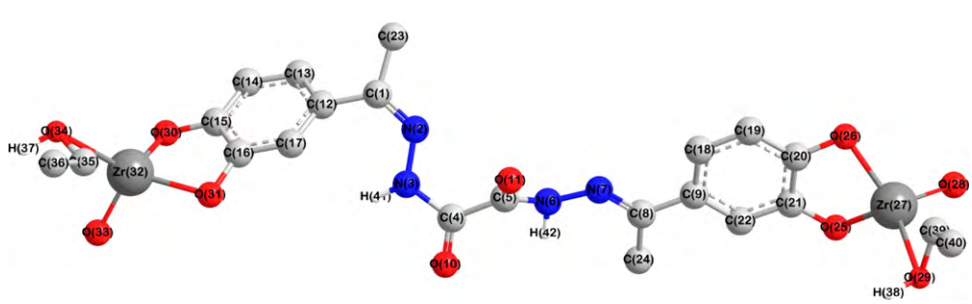

Scheme 6. Molecular modeling of $[(ZrO)_2(H_2L)(C_2H_5OH)_2]$.

Table 4
Effect of some foreign ions on the flotation of 5×10^{-5} mol L^{-1} ZrO^{2+} using 1×10^{-4} mol L^{-1} H_6L and 1×10^{-3} mol L^{-1} HOL at pH ~3.

Cation	Foreign/ZrO^{2+}	F (%)	Anion	Foreign/ZrO^{2+}	F (%)
Na^+	200	99.2	Cl^-	200	99.4
K^+	200	98.4	SO_4^{2-}	20	92.2
Ca^{2+}	200	98.5	Citrate	20	80.0
Co^{2+}	20	99.5	HPO_4^-	20	86.7
Ni^{2+}	20	98.5	CH_3COO^-	20	99.2
Cu^{2+}	20	8.5			
Zn^{2+}	20	75.8			
Cd^{2+}	20	99.5			
NH_4^+	100	98.4			
Al^{3+}	20	74.2			

Table 5
Recovery (*R*%) of ZrO^{2+} ions added to 10 mL of some water samples using 1×10^{-4} mol L^{-1} H_6L and 1×10^{-3} mol L^{-1} HOL at pH ~3.

Type of water (location)	ZrO^{2+} added (mg L^{-1})	*R*%
Tap water (Home lab.)	5.36 10.71	98.998.2
Nile water (Mansoura City)	5.36 10.71	98.898.5
Sea water (Gamasa)	5.36 10.71	98.297.5
Underground water (Belkas city)	5.36 10.71	99.098.5
Lake water (El-Manzala lake)	5.36 10.71	99.697.5

Mn^{2+}, Zn^{2+} Cu^{2+}, Al^{3+}, HPO_4^- and citrate ions. The interference is diminished by adding excess H_6L. Thus, the introduced procedure is fairly selective and can be safely employed for the separation and determination of ZrO^{2+} in various materials.

Ionic strength: The effect of some salts resembled those in natural water samples on the flotation efficiency of 0.5×0^{-4} mol L^{-1} ZrO^{2+} is studied. The ionic strength of the medium has no effect on the flotation process.

Application: To apply the procedure for separation and determination of ZrO^{2+} in water samples taken from different locations, add 5.36 and/or 10.71 ppm of ZrO^{2+} to 10 mL of clear water and adjust the pH to ~3 at 30 °C. After flotation, the concentration of ZrO^{2+} was determined spectrophotometrically using xylenol orange at 535 nm in the mother liquor. From the data in Table 5, ZrO^{2+} is determined with satisfactory results.

4. Conclusion

A new chelating agent has been prepared and characterized. It introduced for chelation with VO^{2+}, ZrO^{2+}, HfO^{2+}, $MoO_2{}^{2+}$ and $UO_2{}^{2+}$ as well as Cr(III). It chelates as a mononegative bidentate and forms mononuclear complexes with the studied metal ions except ZrO^{2+} which forms binuclear complex. The complexes seem to be polymeric in nature due to their insolubility and high melting points. $[Cr(H_4L)(H_2O)_3Cl]\cdot H_2O$, $[HfO(H_4L)(H_2O)]\cdot H_2O$, $[MoO_2(H_4L)]$ and $[UO_2(H_4L)(H_2O)_2]\cdot 2H_2O$ have been proposed to be octahedral; $[(ZrO)_2(H_2L)(C_2H_5OH)_2]$ is four coordination where $[VO(H_4L)(H_2O)_2]$ is square based pyramid. VO^{2+} and Cr(III) complexes degrade the DNA of eukaryotic subject completely. The flotation technique was found applicable for the separation of 0.5×10^{-4} mol L^{-1} ZrO^{2+} ions using 1×10^{-4} mol L^{-1} H_6L and 1×10^{-5} mol L^{-1} oleic acid at pH 3.

Appendix A. Supplementary data

Supplementary data associated with this article can be found, in the online version, at doi:10.1016/j.saa.2010.05.026.

References

[1] J.D. Ranford, J.J. Vittal, Y.M. Wang, Inorg. Chem. 37 (1998) 1226–1231.
[2] D.D. Periin, Topics in Current Chemistry, Springer Verlag, New York, 1976.
[3] A.A. El-Asmy, M.E. Khalifa, M.M. Hassanian, Synth. React. Inorg. Met.-Org. Chem. 31 (2001) 1787–1801.
[4] A.A. El-Asmy, M.E. Khalifa, M.M. Hassanian, Synth. React. Inorg. Met.-Org. Chem. 28 (1998) 873.
[5] Z. Huszti, G. Szihigyi, E. Kasztreiner, Biochem. Pharmacol. 32 (1983) 627–638.
[6] S. Fucharoen, P.T. Rowley, N.W. Paul, Thalassemia: Pathophysiology and Management, Part B, Alan R. Liss, New York, 1998.
[7] T.B. Murphy, N.J. Rose, V. Schomaker, A. Aruffo, Inorg. Chim. Acta 108 (1985) 183–194.
[8] D.K. Johnson, T.B. Murphy, N.J. Rose, W.H. Goodwin, L. Pickart, Inorg. Chim. Acta 67 (1982) 159–163.
[9] M.A. Khattab, M.S. Soliman, G. El-Enany, Bull. Soc. Chim. Belg. 91 (1982) 265–271.
[10] N.M. El-Metwally, A.A. El-Asmy, A.A. Abu-Hussen, Int. J. Pure Appl. Chem. 1 (2006) 75–81.
[11] M.S. Refat, J. Mol. Struct. 842 (2007) 24–37.
[12] P.R. Mandlik, A.S. Aswar, Pol. J. Chem. 77 (2003) 129–135.
[13] A.S. El-Tabl, F.A. El-Saied, W. Plass, A.N. Al-Hakimi, Spectrochim. Acta 71A (2008) 90–99.
[14] O.A. El-Gammal, A.A. El-Asmy, Coord. Chem. 61 (2008) 2296–2306.
[15] A.I. Vogel, Text Book of Quantitative Inorganic Analysis, Longmans, London, 1994.
[16] A.A. El-Asmy, O.A. El-Gammal, D.A. Saad, S.E. Ghazy, J. Mol. Struct. 934 (2009) 9–22.
[17] A.A. El-Asmy, O.A. El-Gammal, H. Saleh, Spectrochim. Acta 71 (2008) 39–44.
[18] S.P. McGlynn, J.K. Smith, J. Chem. Phys. 35 (1961) 105.
[19] L.H. Jones, Spectrochim. Acta 10A (1958) 395–403.
[20] A.A. El-Asmy, M.A. Hafez, E.M. Saad, F.T. Taha, Trans. Met. Chem. 19 (1994) 603–605.
[21] N.M. El-Metwally, R.M. El-Shazly, I.M. Gabr, A.A. El-Asmy, Spectrochim. Acta 61A (2005) 1113–1119.
[22] S.P. McGlynn, J.K. Smith, J. Mol. Spectrosc. 6 (1961) 164–187.
[23] A. Syamal, M. Ram Maurya, Trans. Met. Chem. 11 (1986) 255–258.
[24] T. McMaster, M.D. Garducci, Y.S. Yang, E.I. Solomon, J.H. Enemark, Inorg. Chem. 40 (2001) 687–702.
[25] B.T. Thaker, J. Lekhadia, A. Potel, P. Thaker, Trans. Met. Chem. 19 (1994) 623–631.
[26] S. Khasa, V.P. Seth, P.S. Gahlot, A. Agarwal, R.M. Krishna, S.K. Gupta, Physica B 334 (2003) 347–358.
[27] N. Raman, A. Kulandalsamy, C. Thangaraja, Trans. Met. Chem. 28 (2003) 29–35.
[28] D. Kiverlson, S.K. Lee, J. Chem. Phys. 41 (1964) 1896–1903.
[29] D.U. Warad, C.D. Statish, V.H. Kulkarni, C.S. Bajgur, Ind. J. Chem. 39A (2000) 415–420.
[30] U.B. Gangadharmath, S.M. Annigeri, A.D. Naik, V.K. Revankar, V.B. Mahale, J. Mol. Struct. 572 (2001) 61–71.